Industrial Chemistry & Materials

ROYAL SOCIETY OF CHEMISTRY

PAPER

View Article Online
View Journal | View Issue

Cite this: *Ind. Chem. Mater.*, 2025, **3**, 631

Synergistic strengthening of ion-exchange resins by post-crosslinking and selective sulfonation for PGMEA purification†

Nian Zhang,[ab] Fan Liu,[a] Dan Li,[a] Chunyan Shi,[c] Aizi Cai,[a] Shizhe Xu,[a] Yaocheng Dai,[a] Yan Wang*[b] and Haifeng Dong*[ac]

PGMEA is widely used as a solvent and diluent for photoresists, yet developing an efficient resin that simultaneously resists organic dissolution and removes trace metal ions presents a significant challenge. To overcome this, a novel sulfonated hyper-cross-linked resin (2-CS-DVB-SO_3H) was synthesized through a multi-step process involving the preparation of a Cl-functionalized gel polymer, followed by sulfonation and post-crosslinking. The effects of the monomers, crosslinking degree, sulfonation degree, dosage, adsorption temperature, and resin stability on its purity performance were discussed. The resulting resin demonstrated exceptional stability in organic media and effectively purified PGMEA under optimized conditions (30% crosslinking, 4.69% S content, and 0.2 g mL^{-1} resin dosage), with Ti, Co, Ni, and Cu metal ion concentrations reduced below 10 ppb. This process elevated PGMEA purity from 98.90% to 99.48%. Thermodynamic analysis revealed the adsorption to be non-spontaneous. The resin maintained chemical stability in PGMEA within 18 h. FT-IR and XPS data identified ion exchange, electrostatic interactions and lone electron pair coordination between sulfonic acid groups and metal ions as the binding mechanisms. The hydrogen bonds formed between Cl^- on the resin and hydroxyl groups in methanol (as organic impurities) were considered the primary factor responsible for enhancing the purity of PGMEA. These results collectively establish 2-CS-DVB-SO_3H as a robust and reliable material for metal ion removal in PGMEA purification, thereby improving the purity of photoresist solvents and potentially enhancing photoresist performance.

Received 10th May 2025,
Accepted 18th June 2025

DOI: 10.1039/d5im00078e

rsc.li/icm

Keywords: Sulfonated resin; PGMEA; Metal ion removal; Purification mechanisms.

1 Introduction

Integrated circuit chips, as the cornerstone of the semiconductor industry, are vital for modern electronics, communication, AI, and advanced computing, determining global competitiveness and innovation in the digital economy.[1] Photoresists, comprising resin matrices, photosensitizers, additives, and high-purity solvents, exhibit synergistic interactions that govern critical performance metrics in exposure accuracy, linewidth control, and defect density.[2,3] These photochemical materials further constitute pivotal enablers in extreme ultraviolet (EUV) lithography processes, where they fundamentally determine the production yield and ultimate chip performance in advanced semiconductor manufacturing nodes.[4,5] Propylene glycol monomethyl ether acetate (PGMEA), with its high solubility, excellent thermal stability, low toxicity and minimal corrosion, serves as a critical solvent in the semiconductor manufacturing.[6,7] It is widely used in photoresist formulation, thinners and anti-reflective coatings, with its high-purity properties being essential for EUV lithography and the chip yield.[8] The purity of PGMEA critically determines the spatial uniformity of photochemical conversion efficiency and the substrate wettability dynamics of photoresists, primarily particles and metal ions.[9] Particles formed due to aging, the dilution process, or elevated storage temperatures can be removed by filtration using membranes with pore sizes smaller than the contaminant.[10] Metal ions such as Fe, Cu, Ni, Cr, Co, Pt, and Ir can dissolve into the Si matrix or form silicide, resulting in p–n junction leakage.[11] Moreover, these metal ions degrade gate oxide quality in integrated circuits,

[a] *Huizhou Institute of Green Energy and Advanced Materials, Huizhou, Guangdong 516081, China*
[b] *Advanced Energy Science and Technology Guangdong Laboratory, Huizhou, Guangdong 516003, China*
[c] *CAS Key Laboratory of Green Process and Engineering, Beijing Key Laboratory of Ionic Liquids Clean Process, Institute of Process Engineering, Chinese Academy of Sciences, Beijing 100190, China*

† Electronic supplementary information (ESI) available. See DOI: https://doi.org/10.1039/d5im00078e

altering electrical characteristics.[12] However, removing trace metal ions remains a significant challenge, as even contaminants at parts per billion (ppb) levels can lead to equipment failure.[13]

Currently, organic solvent purification is achieved through various techniques including adsorption processes, reactive distillation, liquid–liquid extraction and membrane separation.[6,14–17] Chaniago *et al.* pioneered a heterogeneous azeotropic dividing-wall column that reduces capital expenditure by 20–30% and energy consumption by 30–40% while achieving >98% recovery of PGME/PGMEA from waste solvents.[18] Lee *et al.* subsequently integrated reactive and pressure-swing distillation (RD-PSD) for PGMEA production, attaining 99.995% purity (<0.1 ppb metal ions) with 25–35% energy savings and 40% enhanced operational flexibility.[19] Compared with other methods, adsorption has emerged as a particularly promising approach due to its distinct advantages, such as cost-effectiveness, high separation efficiency, environment-friendliness and operational simplicity.[20] However, PGMEA contains both an ether bond and a carbonyl group, endowing it with exceptional solvation capability for both polar and non-polar compounds, which can significantly affect the structural stability of conventional adsorbents, such as molecular sieves, polymeric resins, and metal–organic frameworks, when deployed in PGMEA media. The resins exhibit a spherical particle structure, demonstrating chemical resistance to acids, bases and organic solvents. Combined with their facile separation and modification potential, resins are an ideal candidate for organic chemical purification in industrial-scale applications.[21,22] In 1969, Davankov *et al.* first reported the synthesis and properties of hyper-cross-linked polystyrenes, which were synthesized by Friedel–Crafts alkylation of linear or lightly cross-linked polystyrene precursors.[23,24] These resins exhibited superior properties over conventional zones, such as facile synthesis and tailored design enabled by versatile precursor selection, high specific surface area with an optimized pore architecture, and exceptional swelling behavior in both compatible and poor solvents.[25] Additionally, they display tunable surface wettability alongside remarkable thermal and chemical stability.[26] The complex three-dimensional network structure of hyper-cross-linked resins contributes to their unique combination of physicochemical properties, making them particularly attractive for applications requiring robust polymeric matrices with tailored porosity and solvent compatibility.[25]

By introducing specific functional groups into the resin skeleton through chemical modification, the hyper-cross-linked resin can be endowed with new physical and chemical properties. Sulfonic acid makes the resin have a large amount of negative charge, have a strong electrostatic attraction to metal ions, and able to efficiently adsorb a variety of metal ions, and its exchange capacity is much higher than that of carboxylic acid (–COOH) or phosphoric acid ($-PO_3H_2$) resins.[27] Hou *et al.* reported that a dual-functional NSHAR resin (sulfonic acid–thioether synergy) achieved a gold adsorption capacity of 1440 mg g^{-1}, significantly surpassing the <500 mg g^{-1} limit of conventional resins, providing an efficient pathway for low-grade precious metal recovery.[28] Zhang *et al.* employed a styrene-divinylbenzene sulfonic acid resin (1.6 g L^{-1}) to directionally remove >99% Zn^{2+} from BHET, resolving the industry challenge of product discoloration caused by catalyst residues in polyester synthesis.[29] Tan *et al.* synthesized a sulfonated microporous hyper-cross-linked resin, attaining Cu^{2+} adsorption of 51.45 mg g^{-1} at 303 K. Its 3D network structure (specific surface area >1000 m^2 g^{-1}) triples adsorption kinetics, breaking the efficiency barrier for low-temperature operation.[30] Tran *et al.* confirmed the broad-spectrum adsorption capability of sulfonated polystyrene resins for $Zn^{2+}/Cu^{2+}/Cd^{2+}$ (4.09–4.58 mg g^{-1}), with uniform pore structures effectively suppressing ion competition effects.[31] Chang *et al.* prepared strong-acid resin St-DVB-g-ACE-3, elevating the Na^+/K^+ adsorption capacity to 33.3 mg g^{-1} and the trace metal removal to <1 ppb in industrial-grade NMP *via* fixed-bed operation, meeting ultra-pure electronic chemical standards (SEMI C63) for the first time.[32] These innovations in hyper-cross-linked sulfonated resin synthesis—propelled by functional group engineering (*e.g.*, $-SO_3H$/–SR synergy), topological optimization (hierarchical pore design), and process integration (high-flow-velocity fixed beds)—are advancing high-purity chemical manufacturing into a new era.

To address the critical challenges of poor resistance to organic solvents and low metal adsorption efficiency in conventional ion-exchange resins caused by the strong solvation properties of PGMEA, this study innovatively proposed a "post-crosslinking coupled with site-selective sulfonation" strategy, developing a novel resin material that integrates high solvent resistance with efficient ion-exchange capacity. The influence of factors such as the monomer, crosslinking degree, sulfonation degree, resin dosage, adsorption temperature and time was systematically studied to obtain the optimal experimental conditions. The adsorption mechanism was explored by FTIR and XPS. Compared to traditional methods, the synthesized resin significantly enhanced the removal efficiency of trace metal impurities in PGMEA and ensured solvent purity requirements. This work proposed a practical approach for semiconductor photoresist solvent purification, contributing to the development of more reliable and self-sufficient critical materials in advanced chip manufacturing.

2 Results and discussion

2.1 The effect of different monomers on resin performance

The stability and adsorption capacity of resins are critical factors in determining their effectiveness for removing metal ions from PGMEA. On the one hand, the selected resin must exhibit high stability in PGMEA to avoid dissolution, which could compromise solvent purity and introduce additional impurities. On the other hand, excessive crosslinking can lead to overly dense internal structures, hindering the grafting ability of sulfonic acid groups and thereby reducing adsorption performance. Thus, balancing stability and

adsorption capacity is a key challenge in synthesizing resins for PGMEA purification.

The stability evaluation of commercial resins in PGMEA revealed significant material degradation, as demonstrated by decreased solvent purity and substantial weight loss (Fig. S1†). Among these, the Amberlite IR 120 H resin showed relatively better stability than other commercial resins and was selected as a representative comparator, though it still exhibited marked purity degradation upon PGMEA immersion (Table 1). In contrast, our post-crosslinking technology constructed a rigid three-dimensional network through delayed divinylbenzene crosslinking, substantially enhancing the material's resistance to PGMEA degradation. Meanwhile, the selection of sulfonation sites is a crucial strategy for resin performance, particularly adsorption capacity. Table 1 compares the commercial sulfonic acid resin (Amberlite IR 120 H), the post-crosslinking sulfonated resins (St-DVB-SO_3H), and two post-crosslinking resins with different positional sulfonation (4-CS-DVB-SO_3H and 2-CS-DVB-SO_3H). As an electrophilic aromatic substitution reaction, sulfonation reactivity is significantly influenced by both the electronic effects and steric hindrance of substituents on the benzene ring.[33] A comparative study of two chlorinated resins—*para*-chloro-substituted 4-CS-DVB-SO_3H and *ortho*-chloro-substituted 2-CS-DVB-SO_3H—revealed that the chlorine atom (–Cl), as a strong electron-withdrawing group, reduced the electron density of the benzene ring and diminished sulfonation reactivity. More critically, the spatial accessibility of sulfonation sites is heavily affected by the chlorine position: the *para*-chlorophenyl group (4-CS) exhibits significantly greater steric hindrance than the *ortho*-chlorophenyl group (2-CS). This heightened steric obstruction severely impeded the successful grafting of sulfonic acid groups (–SO_3H) onto the benzene ring. The combined electronic and steric effects resulted in a substantially lower degree of sulfonation in the *para*-chloro-substituted resin (4-CS-DVB-SO_3H) compared to its *ortho*-chloro counterpart (2-CS-DVB-SO_3H). Specifically, the sulfur content (S%) plunged from 5.07% in 2-CS-DVB-SO_3H to 2.45% in 4-CS-DVB-SO_3H. Since the sulfur content directly reflected the quantity of key adsorption sites (sulfonic acid groups), suboptimal sulfonation site selection (*e.g.*, using *para*-chloro-substituted monomers) severely compromised the resin's metal ion adsorption capacity. Thus, optimizing the spatial environment of sulfonation sites—such as favouring *ortho*-substituents with lower steric hindrance—is essential for enhancing resin adsorption performance.

The adsorption capacity (dependent on the sulfur content) of the resins for Ti, Fe, Co, Ni, Cu, and Zn metal ions and the purity of PGMEA were used as the main indices to determine the appropriate adsorbent (Fig. 1). The original purity of PGMEA was 98.9%, which was detected using an Agilent 8890 gas chromatograph equipped with an autosampler. The specific detection methods are documented in the ESI.† The PGMEA after purification of the commercial resin decreased to 89.62%, which was considered to be caused by the poor solvent resistance of the resin dissolved in PGMEA. The resin synthesized in this work exhibited greatly improved solubility resistance to PGMEA. Notably, the chlorine-containing resins exhibited better solvent resistance than their chlorine-free counterparts. This was because the introduction of additional –Cl on the benzene can improve the resistance to thermal desulphurization of the sulfonic acid functional group.[34,35] 2-CS-DVB-SO_3H has the strongest adsorption capacity for metal ions, which was the most suitable adsorbent

Table 1 The influence of different monomers on the properties of resins

Resin	Monomer	Crosslinking density (%)	S content (%)
Amberlite IR 120 H	Styrene	8	12.54
St-DVB-SO_3H	Styrene	20	5.07
4-CS-DVB-SO_3H	4-Chlorostyrene	20	2.45
2-CS-DVB-SO_3H	2-Chlorostyrene	20	4.31

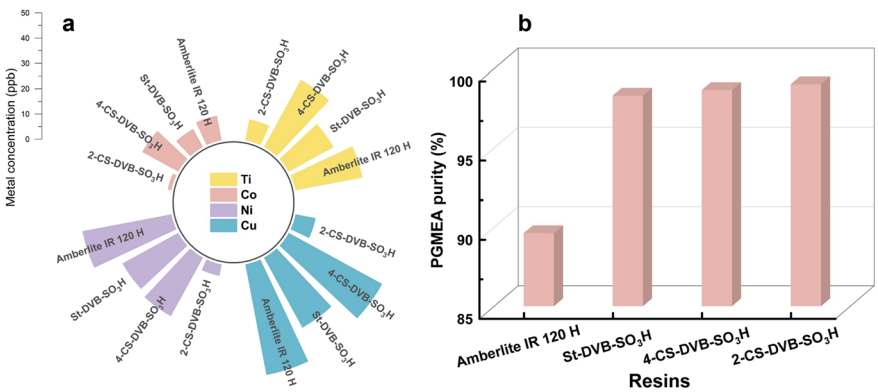

Fig. 1 (a) The concentration of metal ions in PGMEA after adsorption with different resins; (b) the purity of PGMEA after adsorption with different resins.

considering the purity of PGMEA and the concentration of metal ions after adsorption. Therefore, 2-CS-DVB-SO_3H was used in the subsequent experiments.

The scanning electron microscopy-energy dispersive spectroscopy (SEM-EDS) coupling technique was employed to analyze changes in the surface morphology of the synthesized 2-CS-DVB-SO_3H resins and elemental composition. Fig. 2a–d show the SEM images of the gel polymers before and after sulfonation. The surface morphology of the gel polymers remained largely unchanged, demonstrating that the sulfonation process did not induce particle breakage or structural collapse, confirming the high stability of the resin framework. The EDS mapping images of a sulfonated gel polymer shown in Fig. 2e–g revealed uniform distribution of O, C and S throughout the sample, indicating homogeneous incorporation of sulfonic acid groups within the polymer matrix. It was proved that the synthesized sulfonated gel polymer had a uniform distribution of sulfonic acid groups and uniform particles.

2.2 The effect of the crosslinking degree on resin performance

The degree of crosslinking (ρ) is a core parameter determining resin properties, referring to the density of the three-dimensional network structure formed by chemical bonds between polymer chains. A higher crosslinking degree typically enhances the rigidity, heat resistance, chemical stability and mechanical strength of resins.[36–38] In this work, DVB played a cross-linking role, and the amount of DVB used in the synthesis process was regarded as the theoretical degree of cross-linking. As shown in Fig. 3a, the thermal decomposition temperature of the synthesized gel polymers increased from 658 K to 675 K with higher crosslinking density. As shown in Fig. 3b, when the crosslinking degree of 2-CS-DVB-SO_3H was 5%, the purity of PGMEA dropped to 98.12% due to the poor organic dissolution resistance of the low crosslinking resin. As the crosslinking degree was 20%, the purity of PGMEA increased to 99.27%. This was because the highly crosslinked network restricted the movement of molecular chains and the penetration of solvents, which reduced the degree of swelling and solubility.[39,40] The improvement of the crosslinking degree was conducive to the structural stability of the resin. Fig. 3c demonstrates that the 2-CS-DVB-SO_3H resin with 30% crosslinking degree achieves optimal performance, exhibiting the lowest residual concentrations of Ti, Fe, Co, and Cu metal ions while maintaining high PGMEA purity (99.34%). This balance stemmed from its moderately crosslinked structure, which provided sufficient porosity for metal ion diffusion while preserving accessible sulfonic acid groups for effective adsorption. In contrast, increasing the crosslinking degree to 40% enhances resin stability and PGMEA purity (99.54%) but significantly reduced the sulfonic acid group loading (3.99%, Fig. S4†) and metal ion adsorption capacity. This decline

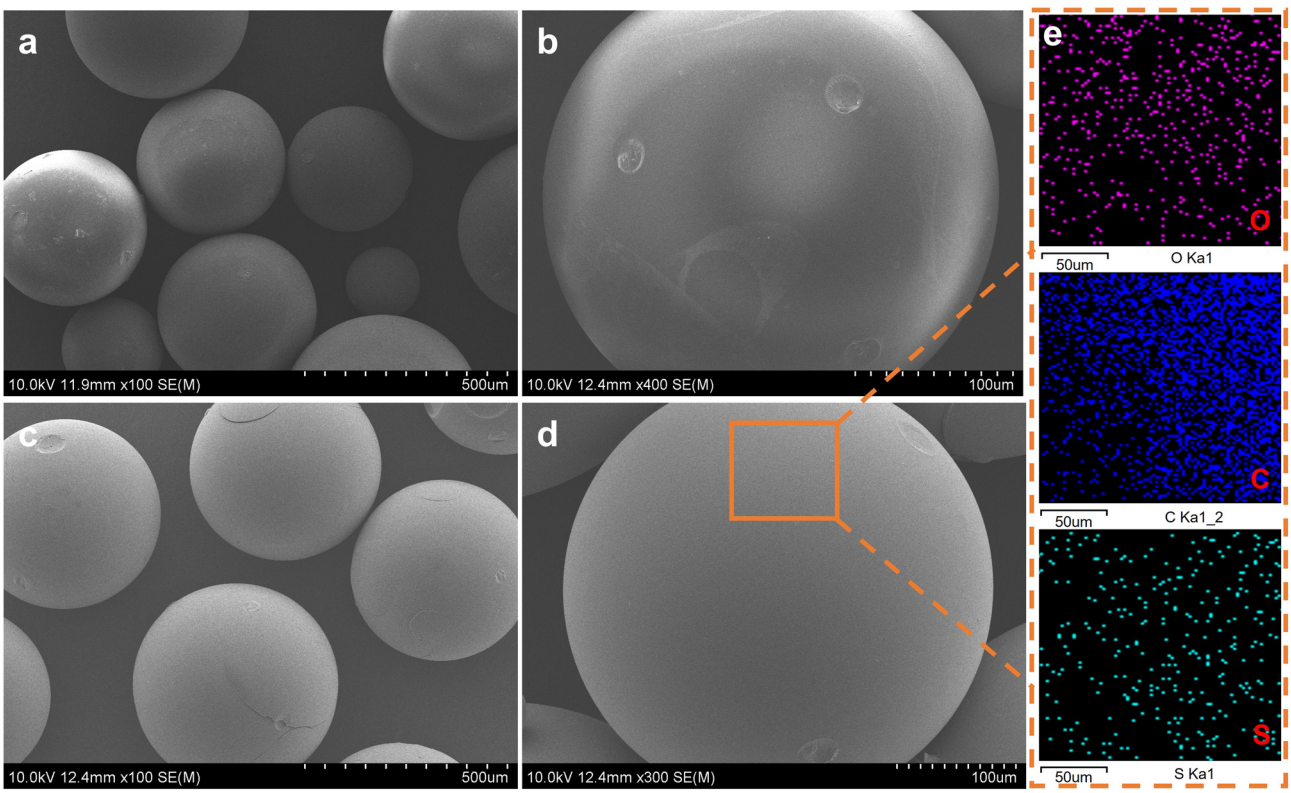

Fig. 2 (a) SEM image of gel polymers with a resolution of 500 μm; (b) SEM image of a gel polymer with a resolution of 100 μm; (c) SEM image of sulfonated gel polymers with a resolution of 500 μm; (d) SEM image of a sulfonated gel polymer with a resolution of 100 μm; (e) EDS mapping images of the sulfonated gel polymer.

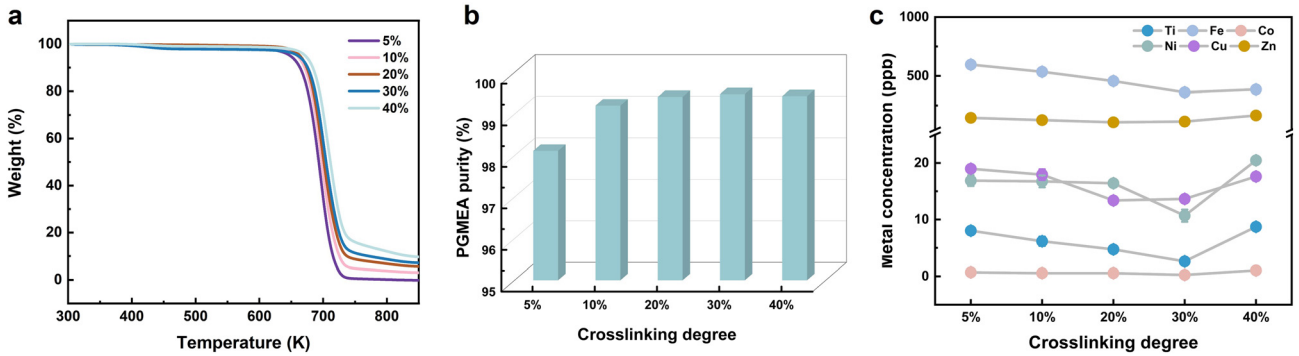

Fig. 3 (a) Thermogravimetric curves of gel polymers at different crosslinking degree; (b) the purity of PGMEA after adsorption with resins at different crosslinking degree; (c) the concentration of metal ions in PGMEA after adsorption with resins at different crosslinking degree.

resulted from excessive network rigidity, which restricted both sulfonic acid grafting (due to steric hindrance) and ion transport (due to limited swelling). Thus, the 30% crosslinked resin represents an optimal compromise, maximizing adsorption efficiency without sacrificing structural integrity, making it the preferred choice for PGMEA purification.

2.3 The influence of sulfonation reagent dosage on adsorption performance

The degree of sulfonation significantly affects the adsorption properties of the resin by altering its chemical and physical structure. The introduction of sulfonic acid groups (–SO_3H) increases the acid site on the surface, enhancing its electrostatic adsorption and ion exchange capacity for metal ions.[41,42] Additionally, the high charge density of the sulfonation resin can enhance the selective adsorption of cations. When synthesizing sulfonated polymers, the amounts of sulfuric acid were 1 mL, 1.5 mL, 2 mL, 2.5 mL and 3 mL with 5 g gel polymers, and the corresponding resin was named 2-CS-DVB-SO_3H-1, 2-CS-DVB-SO_3H-2, 2-CS-DVB-SO_3H-3, 2-CS-DVB-SO_3H-4 and 2-CS-DVB-SO_3H-5, respectively. The S content of the resins increased from 3.84% to 5.21%, and the purity of PGMEA increased from 99.00% to 99.14% after adsorption (Fig. 4a and b). It can be seen from the data in Fig. 4c that the adsorption capacity of Fe, Co, Ni, and Cu metal ions peaked at a sulfuric acid amount of 2.5 mL (S% = 4.69%). When the dosage of sulfuric acid was increased to 3 mL, the adsorption capacity of the resin decreased instead. This is because excessively high sulfuric acid concentrations led to the formation of sulfone bridges between benzene rings. These bridges acted as cross-linking agents, reducing the pore size and the swelling capacity of the resin, lowering the effective sulfonation degree, and thus diminishing the adsorption ability of the resin.[43] Since the degree of sulfonation has a nonlinear relationship with adsorption properties, optimizing the number of active sites and structural stability of the resin is critical.

2.4 The effect of the resin dosage on adsorption performance

The resin dosage is an important factor that influences the adsorption ability, which is critical for practical feasibility and potential applications. The influences of different resin (30% crosslinking degree, 4.69% S content) dosages were investigated to obtain the optimal experimental conditions. As illustrated in Fig. 5, PGMEA was purified with different doses of resin (0.04–0.4 g mL^{-1}), and the adsorption capacity of the resin increased and then decreased. At a resin dosage of 0.2 g mL^{-1}, the highest removal efficiencies (R) were achieved for Ti, Fe, Co, Ni, Cu, and Zn metal ions (87.96%, 66.00%, 81.59%, 51.43%, 79.99%, and 74.87%),

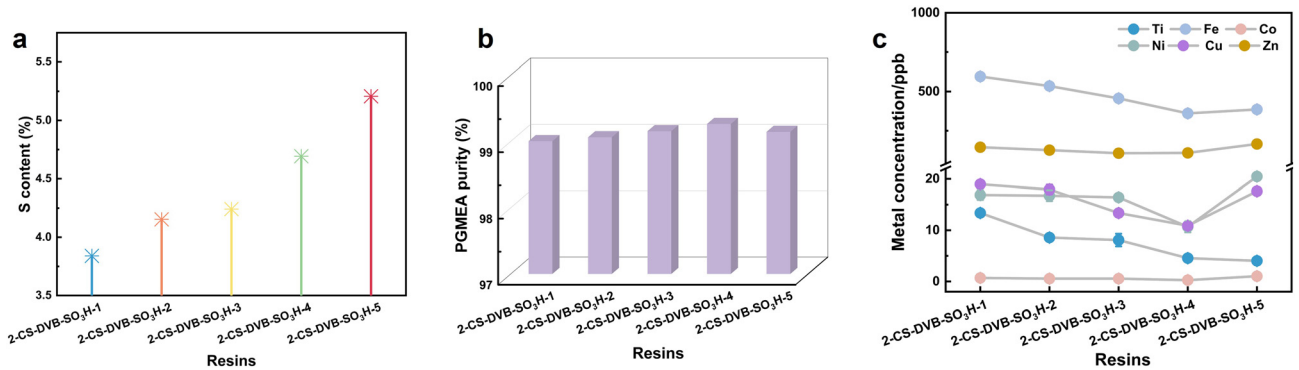

Fig. 4 (a) The S content of resins with different amounts of sulfuric acid; (b) the purity of PGMEA after adsorption of resins with different amounts of sulfuric acid; (c) the concentrations of metal ions in PGMEA after adsorption of resins with different amounts of sulfuric acid.

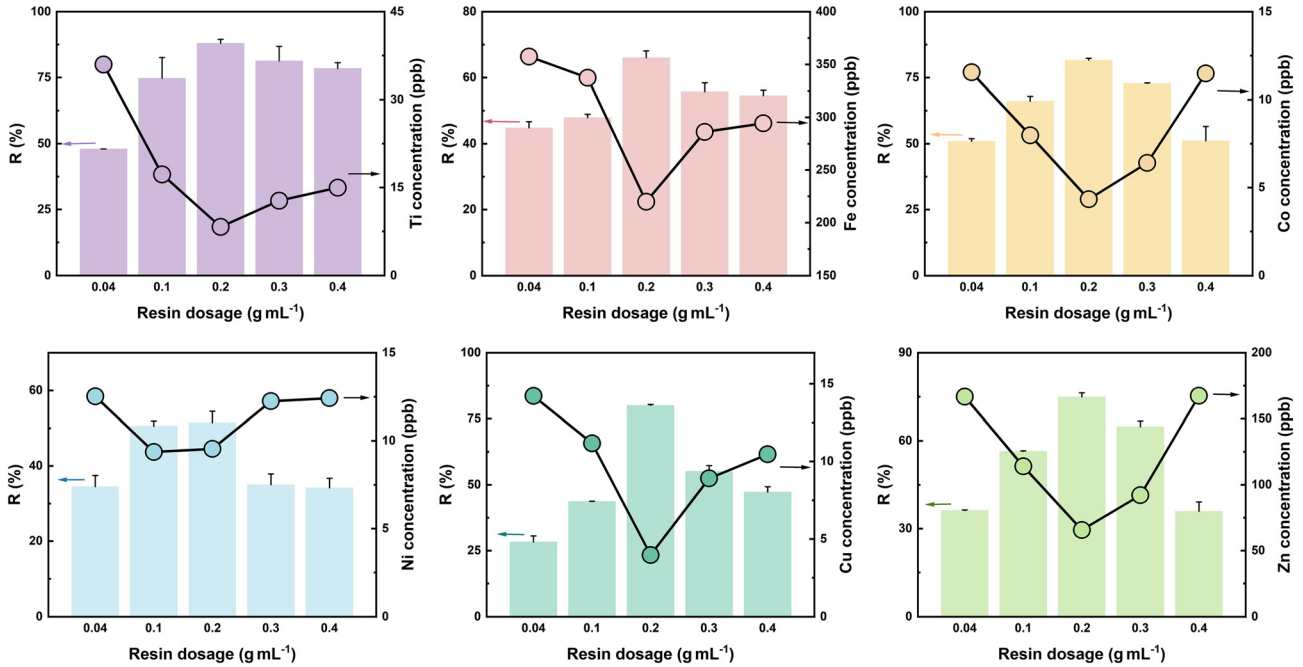

Fig. 5 The concentration and *R* of metal ions in PGMEA which were adsorbed with different amounts of resins.

respectively. The concentrations of Ti, Co, Ni, and Cu metal ions were reduced to below 10 ppb. As shown in Fig. 6a, the purity of PGMEA increased to 99.48%. However, further increasing the resin dosage did not continue to reduce the metal ion concentration or improve the PGMEA purity. This limitation occurs because the resin inherently introduces trace metal impurities into the solvent due to environmental exposure and synthesis processes. While negligible when using small resin quantities with large solvent volumes, these resin-derived impurities significantly impact the overall removal efficiency at higher dosages. Consequently, experimental observations revealed increased metal impurity concentrations and decreased removal efficiency at elevated resin loadings, which is consistent with reported research.[32]

Time has an important influence on the stability of the resin in organic solvents. Based on the above results, the stability experiment of the 2-CS-DVB-SO_3H-4 resin with a dose of 0.2 g mL^{-1} in PGMEA was optimized. The influence of adsorption time on the purity of PGMEA was investigated across various time intervals (0.05–18 h) in Fig. 6b. In the first hour of the experiment, the adsorption of organic impurities by the resin increased, and the purity of PGMEA continuously improved. When the experiment time was 1–18 h, the resin adsorption reached equilibrium, and the purity of PGMEA was maintained between 99.47% and 99.49%. It has been proved that the 2-CS-DVB-SO_3H-4 resin has long-term stability in organic solvents.

2.5 The effect of adsorption temperature

Adsorption thermodynamics provides valuable insight into the exothermic behaviour of metal ions on resins. Adsorption experiments for Ti and Fe metal ions on the resin were carried out at temperatures in the range from 298 K to 328 K.

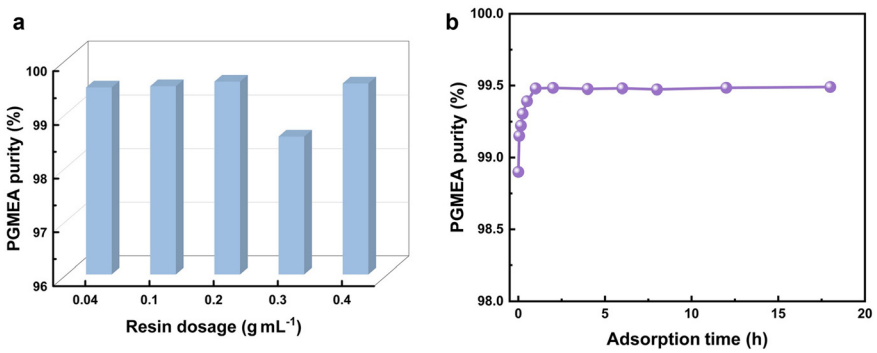

Fig. 6 (a) The purity of PGMEA after adsorption with different amounts of resins; (b) the effect of adsorption time on the purity of PGMEA after resin adsorption.

As can be seen from Fig. 7a, the R of both Ti and Fe metal ions decreased with an increase in temperature. This showed that the elevated temperature adversely affected metal ion adsorption. Correspondingly, the purity of PGMEA was reduced from 99.48% to 98.34%. Fig. 7b demonstrates that the kinetic energy of the resin and solvent will increase as the temperature rises, promoting the diffusion and dissolution of resin chain segments in organic solvents. Therefore, considering both energy efficiency and product preservation, maintaining the adsorption process at room temperature represented the optimal approach.

The R of Ti and Fe metal ions was calculated by formula (1). The thermodynamic parameters of this process, for instance the enthalpy change (ΔH), Gibbs free energy change (ΔG) and entropy change (ΔS), can reveal the integrated thermodynamic behavior at the reaction interface. The thermodynamic parameters were calculated by the following formulas (2)–(5).

$$R = \frac{C_0 - C_e}{C_0} \times 100\% \quad (1)$$

$$Q_e = (C_0 - C_e)\frac{V}{m} \quad (2)$$

$$K_d = \frac{Q_e}{C_e} \quad (3)$$

$$\ln K_d = \frac{\Delta S}{R} - \frac{\Delta H}{RT} \quad (4)$$

$$\Delta G = -RT \ln K_d \quad (5)$$

where R is the removal efficiency of metal ions in PGMEA with resin. The initial and equilibrium metal ion concentrations in PGMEA are C_0 and C_e (mg L^{-1}), the equilibrium metal ion capacity on the resin is Q_e (mg g^{-1}), the volume of the feeding solution is V (L), and the resin dosage is m (g). T (K) is the absolute temperature, R is the universal gas constant (8.314 J mol^{-1} K^{-1}), and K_d is the distribution coefficient of the resin. The thermodynamic results of the adsorption process are listed in Table 2. All the results of ΔG revealing the metal ions on the resin were non-spontaneous and thermodynamically disadvantageous. The endothermic nature of the adsorption process was confirmed by the negative ΔH. Furthermore, the negative value of ΔS showing the extraction process was accompanied by a decrease in the random nature.

3 PGMEA purification mechanism

FT-IR spectroscopy was employed to investigate the adsorption mechanism. As shown in Fig. 8a, the characteristic absorption peaks observed at 1473–1438 cm^{-1}, 2921 cm^{-1} and 682 cm^{-1} can be assigned to C–H bending vibration in benzene rings, C–H stretching vibration and C–Cl stretching vibration, respectively.[44–46] New peaks appeared at 3355 cm^{-1}, 1120 cm^{-1} and 1312 cm^{-1} for the 2-CS-DVB-SO_3H resin, which belong to O–H, S–O and S═O stretching vibration, respectively. The stronger vibrational intensity of the single bond (S–O) compared to the double bond (S═O) agreed with theoretical predictions, confirming the successful introduction of –SO_3H groups.[21,47] The FT-IR spectrum of the resin after adsorption exhibited distinct changes compared to the free resin. Notably, the reduction in the –OH peak intensity at 3355 cm^{-1} suggested that sulfonic acid groups (–SO_3H) likely participated in ion exchange with metal ions in PGMEA. Concurrently, the attenuation of S–O (1120 cm^{-1}) and S═O (1312 cm^{-1}) vibrational peaks and a certain degree of redshift indicated that the deprotonated –SO_3^- groups coordinated with metal ions through coordination.[48] These spectral modifications collectively demonstrated that metal ion adsorption occurred *via* two mechanisms: (1) ion exchange involving proton displacement from –SO_3H groups and (2) coordination between metal cations and the anionic –SO_3^- sites on the resin.

To further investigate the metal ion removal mechanism, the local chemical environments of metal ions adsorbed with resin were analyzed using XPS. Fig. 8b presents the XPS wide scan spectra of 2-CS-DVB-SO_3H before and after metal ion adsorption from PGMEA. Following adsorption, decreased binding energies of O 1s and S 2p orbitals were observed. As shown in Fig. 8c, the high-resolution C 1s spectrum before adsorption could be

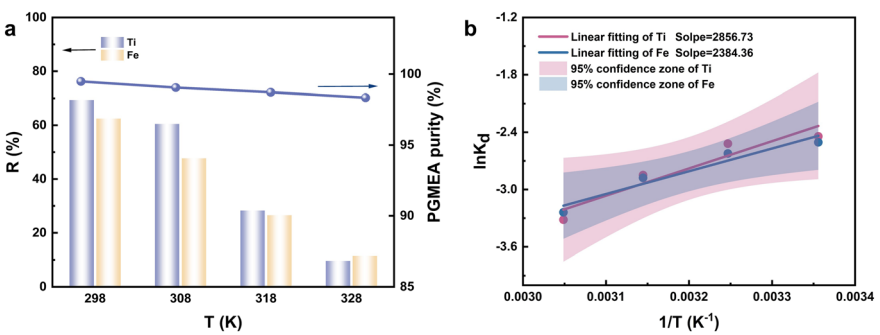

Fig. 7 (a) Effect of temperature on metal ion removal efficiency and purity of PGMEA after resin adsorption; (b) the curve of the thermodynamic model for metal ion adsorption onto resin.

Table 2 The thermodynamic parameters of metal ion adsorption onto resin

	T (K)	ΔG (kJ mol^{-1})	ΔH (kJ mol^{-1})	ΔS (kJ mol^{-1} K^{-1})	R^2
Ti	298	6.09	−23.77	−0.099	0.901
	308	6.45			
	318	7.53			
	328	9.04			
Fe	298	6.21	−19.82	−0.087	0.940
	308	6.72			
	318	7.61			
	328	8.83			

deconvoluted into three characteristic peaks corresponding to C–C/C=C (284.80 eV), C–S (286.12 eV), and C–Cl (287.37 eV), respectively. After adsorption, significant changes occurred where the C–Cl peak decreased to 288.89 eV, probably due to the formation of hydrogen bonds between Cl and the methanol in PGMEA.[49,50] Fig. 8d displays the high-resolution O 1s spectrum before adsorption, which could be deconvoluted into two peaks at 532.43 and 533.69 eV, corresponding to –OH and S=O from the sulfonic acid group in the resin, respectively. After adsorption, the binding energy of S=O/S–O shifted from 533.69 to 532.83 eV, suggesting lone electron pair donation from oxygen to metal ions. The binding energy of –OH shifted from 532.43 to 532.06 eV, which confirmed ion exchange during the adsorption process.[51] The S 2p high resolution spectrum (Fig. 8e) revealed the characteristic spin orbit doublets of –SO_3H, with S $2p_{1/2}$ decreasing from 170.29 to 169.65 eV and S $2p_{3/2}$ shifting from 169.14 to 168.85 eV after adsorption.[52] The analysis results of FT-IR and XPS data consistently prove that there is a synergistic effect of ion exchange and coordination between metal ions and –SO_3H.[53]

4 Conclusion

The synthesized 2-CS-DVB-SO_3H resin demonstrated excellent PGMEA purification capability through efficient metal ion removal, with optimal performance achieved at 30% crosslinking degree, 4.69% S content, and 0.2 g mL^{-1} resin dosage, showing removal efficiencies of 87.96% (Ti), 66.00% (Fe), 81.59% (Co), 51.43% (Ni), 79.99% (Cu), and 74.87% (Zn) while reducing Ti, Co, Ni and Cu metal ions to <10 ppb, and the purity of PGMEA increased from 99.89% to 99.48%. Characterization studies revealed that the chlorine-containing resin exhibited superior stability and adsorption

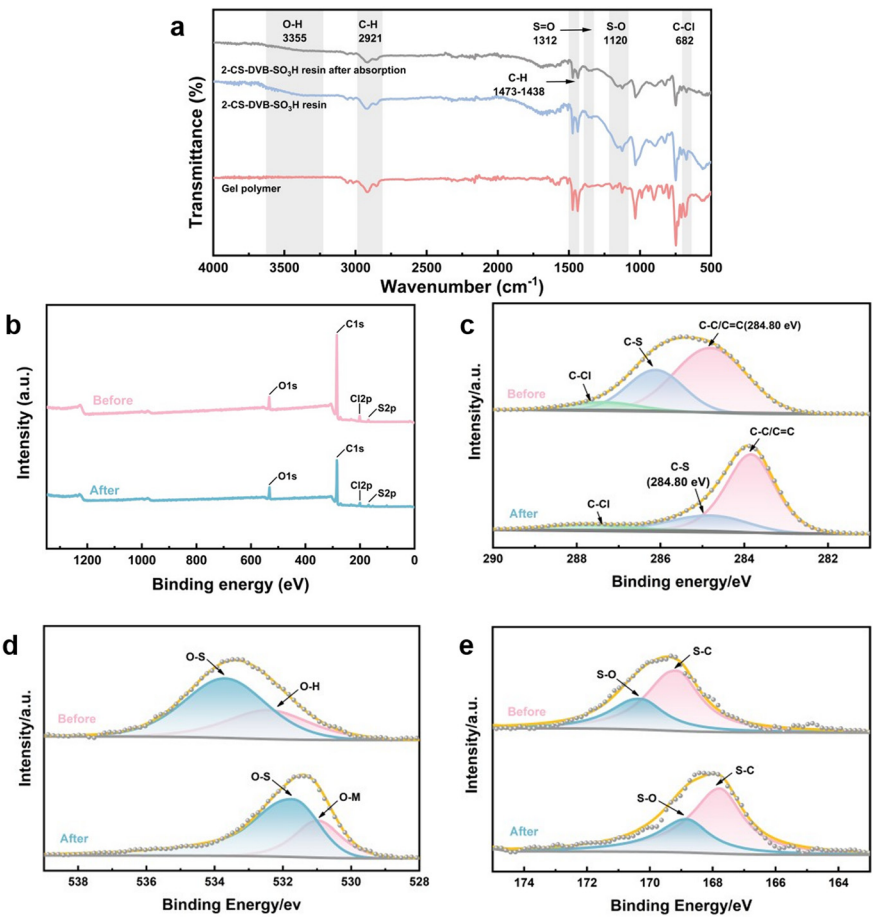

Fig. 8 (a) FT-IR spectra of polymers; (b) XPS full spectrum scan of the resin before and after adsorption; high-resolution XPS spectra of (c) C 1s, (d) O 1s and (e) S 2p before and after adsorption.

capacity compared to other synthetic monomers, with thermodynamic analysis confirming non-spontaneous adsorption that was negatively impacted by temperature increases. The 2-CS-DVB-SO_3H resin can still maintain chemical stability after 18 h. FT-IR and XPS analysis provided mechanistic insights, showing decreased hydroxyl and S═O/S–O peak intensities indicative of ion exchange and electrostatic interactions between sulfonic acid groups and metal ions, along with XPS evidence of electron sharing between S═O oxygen lone pairs and metal ions. Besides, the hydrogen bonds formed between Cl^- on the resin and hydroxyl groups in methanol (as organic impurities) are considered the primary factor responsible for enhancing the purity of PGMEA. Jointly establishing 2-CS-DVB-SO_3H was an effective and stable adsorbent for improving PGMEA purity. It provides a promising method for the purification and separation of wet electronic chemicals.

5 Experimental section

5.1 Materials

2-Chlorostyrene (98%), aluminum chloride (99%), 1,2-dichloroethane (99.5%), and 2,2′-azobis(2-methylpropionitrile) (98%) were purchased from Shanghai Macklin Biochemical Co., Ltd. Propylene glycol monomethyl ether acetate, divinylbenzene (80%), 4-chlorostyrene (97.5%), styrene (99%) and poly(vinyl alcohol) (alcoholysis degree 87.0–89.0%) were obtained from Shanghai Aladdin Biochemical Technology Co., Ltd. Ethanol (AR) and methanol (AR) were purchased from Sinopharm Chemical Reagent Co., Ltd. Sodium hydroxide was obtained from Xilong Scientific Co., Ltd. Sulfuric acid was obtained from Guangzhou Chemical Reagent Factory. The Amberlite IR 120 H ion exchange resin was received from Sigma-Aldrich Co., Ltd.

5.2 Synthesis of resins

5.2.1 Removal of inhibitor TBC. 2-Chlorostyrene, 4-chlorostyrene, styrene and divinylbenzene contain the inhibitor TBC. To remove it, the monomer was reacted with 5% NaOH solution three times and then washed with deionized water until neutral. Finally, the monomers were dried overnight with anhydrous sodium sulfate at 333 K.

5.2.2 Synthesis of gel polymers. 0.02 mol 2-chlorostyrene (2-CS) or 4-chlorostyrene (4-CS) was mixed with 0.02 mol styrene (St) and 0.08 mol divinylbenzene (DVB), respectively. 0.5% (w/w) initiator 2,2′-azobis(2-methylpropionitrile) (AIBN) was added. In the stirring state, 1 g polyvinyl alcohol (PVA) was uniformly added to 100 mL of ultrapure water and heated at a constant speed to 368 K. The dispersed phase was obtained after cooling to room temperature. The organic phase was added to a disperser at a speed of 150 rpm. The reaction was initiated by heating to 333 K for 4 h, followed by further heating to 368 K for 2 h. After the reaction, the product was washed sequentially with methanol, ethanol and ultra-pure water, and dried overnight at 333 K in a blast drying oven.

5.2.3 Sulfonation reaction. 5 g of the gel polymer was immersed in 50 mL 1,2-dichloroethane (EDC) for 2 h. Then, 0.3 g aluminum chloride ($AlCl_3$) and 2 mL sulfuric acid (H_2SO_4) were added. The reaction proceeded at a stirring speed of 200 rpm and a temperature of 383 K for 4 h. After the reaction, the product was washed sequentially with methanol, ethanol and ultrapure water, and then dried overnight at 333 K in a blast drying oven.

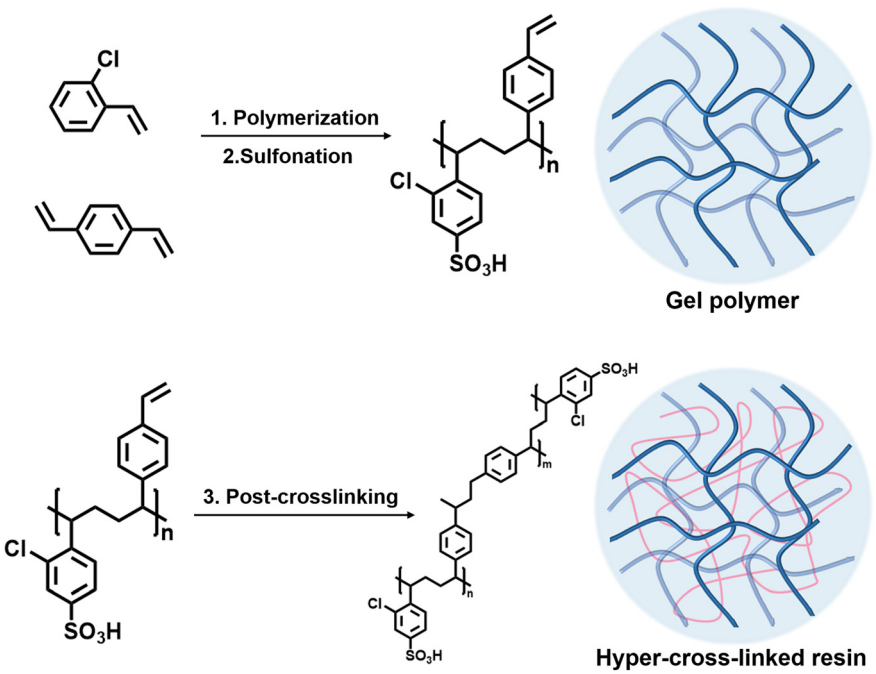

Scheme 1 The complete synthesis route of 2-CS-DVB-SO_3H.

5.2.4 Post-crosslinking reaction. The sulfonated polymers were immersed in 50 mL of EDC for 2 h, followed by the addition of 0.5 g of $AlCl_3$. The reaction was carried out at a stirring speed of 200 rpm and kept at 358 K for 2 h. After that, the product was washed sequentially with methanol, ethanol and ultrapure water, and then dried overnight at 333 K in a blast drying oven. The resin synthesized from 2-CS was designated as 2-CS-DVB-SO_3H, whereas the one derived from 4-CS was labelled 4-CS-DVB-SO_3H. For comparison, St-DVB-SO_3H was prepared using an analogous procedure, with styrene replacing chlorostyrene as the monomer. The complete synthesis route of the 2-CS-DVB-SO_3H resin is shown in Scheme 1.

5.3 Characterization

The FT-IR spectra of polymers in the wavelength range from 4000 cm^{-1} to 400 cm^{-1} were obtained using a Thermo Scientific IS50 FT-IR spectrometer in attenuated total reflection mode. To investigate the microscopic morphology and element distribution, scanning electron microscopy and energy dispersive X-ray spectroscopy elemental mapping imaging were performed utilizing a Hitachi S-4800 at an accelerating voltage of 20 kV. The polymer surface was irradiated using a Thermo Scientific K-Alpha X-ray photoelectron spectrometer with an energy range of 0–1250 eV. A Mettler Toledo thermogravimetric analyzer tested the thermal stability of polymers under the following conditions: heating from 303 K to 1073 K under nitrogen at a rate of 283 K min^{-1}. Using Elementar Vario EL elemental analysis, the sulfur content in the samples was ascertained in the CHNS mode at 1423 K. The purity of PGMEA was assessed using the FID of an Agilent 8890 gas chromatograph (the chromatographic column is HP-PLOT/Q+PT). The concentration of metal ions was determined using an Agilent 8900 triple quadrupole inductively coupled plasma mass spectrometer.

Data availability

The data that support the findings of this study are available from the corresponding authors upon reasonable request.

Author contributions

Nian Zhang, Yan Wang and Haifeng Dong designed the research, analyzed the data and wrote the paper. Nian Zhang performed the research. Fan Liu, Dan Li, Aizi Cai, Shizhe Xu, and Yaocheng Dai participated in data collection and discussion. Chunyan Shi revised the paper.

Conflicts of interest

The authors declare that they have no known competing financial interests or personal relationships that could have appeared to influence the work reported in this paper.

Acknowledgements

This work was supported by the National Key Research and Development Program of China (No. 2020YFA0710204), the Strategic Priority Research Program of the Chinese Academy of Sciences (No. XDA0390503) and the National Natural Science Foundation of China (No. 22278408).

References

1 X. Wang, P. Tao, Q. Wang, R. Zhao, T. Liu, Y. Hu, Z. Hu, Y. Wang, J. Wang, Y. Tang, H. Xu and X. He, Trends in photoresist materials for extreme ultraviolet lithography: A review, *Mater. Today*, 2023, **67**, 299–319.
2 Z. Tang, X. Guo, H. Wang, H. Chen and W. Kang, A new metallization method of modified tannic acid photoresist patterning, *Ind. Chem. Mater.*, 2024, **2**, 284–288.
3 J. Liu, K. Ren, H. Zhao, D. Wang, Q. Wang, Y. Li, X.-D. Xu and W. Kang, Design of dual-sensitive functional photoresist for UV lithography, *ACS Appl. Polym. Mater.*, 2025, **7**, 3103–3111.
4 L.-T. Tseng, P. Karadan, D. Kazazis, P. C. Constantinou, T. J. Z. Stock, N. J. Curson, S. R. Schofield, M. Muntwiler, G. Aeppli and Y. Ekinci, Resistless EUV lithography: Photon-induced oxide patterning on silicon, *Sci. Adv.*, 2023, **9**, 5997.
5 F. Feng, Y. Liu, K. Zhang, H. Yang, B.-R. Hyun, K. Xu, H.-S. Kwok and Z. Liu, High-power AlGaN deep-ultraviolet micro-light-emitting diode displays for maskless photolithography, *Nat. Photonics*, 2025, **19**, 101–108.
6 A. Hussain, Y. D. Chaniago, A. Riaz and M. Lee, Process design alternatives for producing ultra-high-purity electronic-grade propylene glycol monomethyl ether acetate, *Ind. Eng. Chem. Res.*, 2019, **58**, 2246–2257.
7 G. Maldonado, E. Delzell, R. W. Tyl and L. E. Sever, Occupational exposure to glycol ethers and human congenital malformations, *Int. Arch. Occup. Environ. Health*, 2003, **76**, 405–423.
8 P. de Ketttenis, The historic and current use of glycol ethers: A picture of change, *Toxicol. Lett.*, 2005, **156**, 5–11.
9 X. Wang, Y. Peng, X. Wang, l. Zhu and H. Chen, Spatial uniformity assessment of particles distributed in a spherical fuel element using a non-destructive approach, *Sci. Rep.*, 2019, **9**, 7885.
10 N. Khirouni, A. Charvet, D. Thomas and D. Bémer, Regeneration of dust filters challenged with metallic nanoparticles: Influence of atmospheric aging, *Process Saf. Environ. Prot.*, 2020, **138**, 1–8.
11 M. D. Allendorf, R. Dong, X. Feng, S. Kaskel, D. Matoga and V. Stavila, Electronic devices using open framework materials, *Chem. Rev.*, 2020, **120**, 8581–8640.
12 J.-L. Baltzinger and B. Delahaye, Contamination monitoring and analysis in semiconductor manufacturing, *Semicond. Technol.*, 2010, 57–78.
13 T. M. Lammens, M. C. R. Franssen, E. L. Scott and J. P. M. Sanders, Synthesis of biobased N-methyl pyrrolidone by one-pot cyclization and methylation of γ-aminobutyric acid, *Green Chem.*, 2010, **12**, 1430–1436.

14 K. Abels, A. B. Botelho Junior, X. Chen and W. A. Tarpeh, Ligand content and driving force effects on ion-ion permselectivity in ligand-functionalized membranes, *J. Membr. Sci.*, 2025, **714**, 123418.
15 L. Yuan, C. Wang, H. Yang, P. Ning and H. Cao, Hierarchically-porous resin for the adsorption of organic matter in raffinate produced by solvent extraction from the vanadium industry, *Sep. Purif. Technol.*, 2025, **358**, 130383.
16 S. I. G. P. Mohamed, A. A. Shamsabadi, S. Kavousi, M. D. Firouzjaei, M. Elliott, S. Yazdanparast, S. Nejati, M. A. Zaeem and M. Bavarian, Metal Ions removal from organic solvents using MXene-based membranes, *ACS Appl. Eng. Mater.*, 2023, **1**, 2452–2457.
17 D. Ciceri, J. M. Perera and G. W. Stevens, A study of molecular diffusion across a water/oil interface in a Y–Y shaped microfluidic device, *Microfluid. Nanofluid.*, 2011, **11**, 593–600.
18 Y. D. Chaniago, G. R. Harvianto, A. Bahadori and M. Lee, Enhanced recovery of PGME and PGMEA from waste photoresistor thinners by heterogeneous azeotropic dividing-wall column, *Process Saf. Environ. Prot.*, 2016, **103**, 413–423.
19 Y. D. Chaniago, A. Hussain, R. Andika and M. Lee, Reactive pressure-swing distillation toward sustainable process of novel continuous ultra-high-purity electronic-grade propylene glycol monomethyl ether acetate manufacture, *ACS Sustainable Chem. Eng.*, 2019, **7**, 18677–18689.
20 A. Bashir, L. A. Malik, S. Ahad, T. Manzoor, M. A. Bhat, G. N. Dar and A. H. Pandith, Removal of heavy metal ions from aqueous system by ion-exchange and biosorption methods, *Environ. Chem. Lett.*, 2019, **17**, 729–754.
21 Y. E. Ghoussoub, H. M. Fares, J. D. Delgado, L. R. Keller and J. B. Schlenoff, Antifouling ion-exchange resins, *ACS Appl. Mater. Interfaces*, 2018, **10**, 41747–41756.
22 O. Tavakoli, V. Goodarzi, M. R. Saeb, N. M. Mahmoodi and R. Borja, Competitive removal of heavy metal ions from squid oil under isothermal condition by CR11 chelate ion exchanger, *J. Hazard. Mater.*, 2017, **334**, 256–266.
23 V. A. Davankov and M. P. Tsyurupa, Structure and properties of hypercrosslinked polystyrene-the first representative of a new class of polymer networks, *React. Polym.*, 1990, **13**, 27–42.
24 A. V. Pastukhov, M. P. Tsyurupa and V. A. Davankov, Hypercrosslinked polystyrene: A polymer in a non-classical physical state, *J. Polym. Sci., Polym. Phys. Ed.*, 1999, **37**, 2324–2333.
25 S. Xu, Y. Luo and B. Tan, Recent development of hypercrosslinked microporous organic polymers, *Macromol. Rapid Commun.*, 2013, **34**, 471–484.
26 M. P. Tsyurupa and V. A. Davankov, Porous structure of hypercrosslinked polystyrene: State-of-the-art mini-review, *React. Funct. Polym.*, 2006, **66**, 768–779.
27 K. H. Shah, N. S. Shah, G. A. Khan, S. Sarfraz, J. Iqbal, A. Batool, A. Jwuiyad, S. Shahida, C. Han and M. Wawrzkiewicz, The Cr(III) exchange mechanism of macroporous resins: The effect of functionality and chemical matrix, and the statistical verification of ion exchange data, *Water*, 2023, **15**, 3655.
28 K. Hou, X. Xu, Y. Xiang, X. Chen, S. S. Lam, M. Naushad, C. Sonne and S. Ge, Rapid uptake of gold ions by sulfonated humic acid modified phenolic resin with high adsorption capacity and selectivity, *Adv. Compos. Hybrid Mater.*, 2023, **6**, 77.
29 Q. Zhang, R. Huang, H. Yao, X. Lu, D. Yan and J. Xin, Removal of Zn^{2+} from polyethylene terephthalate (PET) glycolytic monomers by sulfonic acid cation exchange resin, *J. Environ. Chem. Eng.*, 2021, **9**, 105326.
30 B. Li, F. Su, H.-K. Luo, L. Liang and B. Tan, Hypercrosslinked microporous polymer networks for effective removal of toxic metal ions from water, *Microporous Mesoporous Mater.*, 2011, **138**, 207–214.
31 A. T. K. Tran, T. T. Pham, Q. H. Nguyen, N. T. T. Hoang, D. T. Bui, M. T. Nguyen, M. K. Nguyen and B. V. der Bruggen, From waste disposal to valuable material: Sulfonating polystyrene waste for heavy metal removal, *J. Environ. Chem. Eng.*, 2020, **8**, 104302.
32 Z. Chang, W. Guo, C. Yang, C. Ye, Q. Wang, B. Li, Y. Xiao, J. Chen and T. Qiu, Removal of trace Na and K metal ions by resin-grafted crown ether for electronic-grade N-methyl pyrrolidone purification, *Sep. Purif. Technol.*, 2025, **356**, 129839.
33 P. F. Siril, H. E. Cross and D. R. Brown, New polystyrene sulfonic acid resin catalysts with enhanced acidic and catalytic properties, *J. Mol. Catal. A: Chem.*, 2008, **279**, 63–68.
34 J. Wolska and J. Walkowiak-Kulikowska, On the sulfonation of fluorinated aromatic polymers: Synthesis, characterization and effect of fluorinated side groups on sulfonation degree, *Eur. Polym. J.*, 2020, **129**, 109635.
35 A. Orjuela, A. J. Yanez, A. Santhanakrishnan, C. T. Lira and D. J. Miller, Kinetics of mixed succinic acid/acetic acid esterification with Amberlyst 70 ion exchange resin as catalyst, *Chem. Eng. J.*, 2012, **188**, 98–107.
36 C. Li and A. Strachan, Molecular simulations of crosslinking process of thermosetting polymers, *Polymer*, 2010, **51**, 6058–6070.
37 Y. Du, G. Zhao, G. Shi, Y. Wang, W. Li and S. Ren, Effect of crosslink structure on mechanical properties, thermal stability and flame retardancy of natural flavonoid based epoxy resins, *Eur. Polym. J.*, 2022, **162**, 110898.
38 Y. Shudo, A. Izumi, K. Hagita, T. Nakao and M. Shibayama, Structure-mechanical property relationships in crosslinked phenolic resin investigated by molecular dynamics simulation, *Polymer*, 2017, **116**, 506–514.
39 Y. Feng, H. Qiu, P. Deng, Z. Nie, J. Chen, K. Gong, X. Fan and S. Qi, Tuning the static and dynamic properties of epoxy vitrimers through modulation of cross-link density, *Eur. Polym. J.*, 2023, **196**, 112308.
40 D. M. Kroll and S. G. Croll, Influence of crosslinking functionality, temperature and conversion on heterogeneities in polymer networks, *Polymer*, 2015, **79**, 82–90.
41 B. D. Bowes, H. Koku, K. J. Czymmek and A. M. Lenhoff, Protein adsorption and transport in dextran-modified ion-exchange media. I: Adsorption, *J. Chromatogr. A*, 2009, **1216**, 7774–7784.

42 Y. Gao, Z. Zhang, S. Zhong and R. Daneshfar, Preparation and application of aromatic polymer proton exchange membrane with low-sulfonation degree, *Int. J. Chem. Eng.*, 2020, **2020**, 1–9.
43 C. Dalla Valle, M. Zecca, F. Rastrelli, C. Tubaro and P. Centomo, Effect of the sulfonation on the swollen state morphology of styrenic cross-linked polymers, *Polym. J.*, 2020, **12**, 600.
44 L. Yang, Y. Li, X. Jin, Z. Ye, X. Ma, L. Wang and Y. Liu, Synthesis and characterization of a series of chelating resins containing amino/imino-carboxyl groups and their adsorption behavior for lead in aqueous phase, *Chem. Eng. J.*, 2011, **168**, 115–124.
45 S. Xiang, H. Mao, W. Geng, Y. Xu and H. Zhou, Selective removal of Sr(II) from saliferous radioactive wastewater by capacitive deionization, *J. Hazard. Mater.*, 2022, **431**, 128591.
46 Y. Ge, S. Zhu, K. Wang, F. Liu, S. Zhang, R. Wang, S.-H. Ho and J.-S. Chang, One-step synthesis of a core-shell structured biochar using algae (Chlorella) powder and ferric sulfate for immobilizing Hg(II), *J. Hazard. Mater.*, 2024, **469**, 133991.
47 Q. Hu, Y. Meng, T. Sun, Q. Mahmood, D. Wu, J. Zhu and G. Lu, Kinetics and equilibrium adsorption studies of dimethylamine (DMA) onto ion-exchange resin, *J. Hazard. Mater.*, 2011, **185**, 677–681.
48 J. Li, Q. Fan, Y. Wu, X. Wang, C. Chen, Z. Tang and X. Wang, Magnetic polydopamine decorated with Mg–Al LDH nanoflakes as a novel bio-based adsorbent for simultaneous removal of potentially toxic metals and anionic dyes, *J. Mater. Chem. A*, 2022, **11**, 461.
49 X. Li, Y.-Y. Cui, Y.-J. Chen, C.-X. Yang and X.-P. Yan, Facile synthesis of dual-functionalized microporous organic network for efficient removal of cationic dyes from water, *Microporous Mesoporous Mater.*, 2020, **296**, 110013.
50 D. Wang, Y. Zhao and Q. Jia, Construction of magnetic sulfonic-functionalized hypercrosslinked polymers for efficient adsorption of azole fungicides from water, *Sep. Purif. Technol.*, 2025, **354**, 128810.
51 Y. Ke, L. Lin, G. Zhang, H. Hong and C. Yan, Aging behavior and leaching characteristics of microfibers in landfill leachate: Important role of surface mesh structure, *J. Hazard. Mater.*, 2024, **470**, 134092.
52 J. Zhang, K. Dong, W. Luo and H. Guan, Catalytic upgrading of carbohydrates into 5-ethoxymethylfurfural using SO_3H functionalized hyper-cross-linked polymer based carbonaceous materials, *Fuel*, 2018, **234**, 664–673.
53 Y. Sun, Y. Gu and J. Yang, Adsorption of N-heterocyclic compounds from aqueous solutions by sulfonic acid-functionalized hypercrosslinked resins in batch experiments, *Chem. Eng. J.*, 2022, **428**, 131163.